Multiconformational analysis of tripeptides upon consideration of implicit and explicit hydration effects

Belén Hernández, Fernando Pflüger, Sergei G. Kruglik, Mahmoud Ghomi

Multiconformational analysis of tripeptides upon consideration of implicit and explicit hydration effects

Belén Hernández [a,b], Fernando Pflüger[b], Sergei G. Kruglik[c], Mahmoud Ghomi[a,b*]

[a]Laboratoire Matrice Extracellulaire et Dynamique Cellulaire (MEDyC), UMR 7369, Université de Reims, Faculté des Sciences, Moulin de la Housse, 51687 Reims Cedex 2, France

[b]Université Sorbonne Paris Nord, UFR Santé-Médecine-Biologie Humaine, Groupe de Biophysique Moléculaire, 74 Rue Marcel Cachin, 93017 Bobigny cedex, France

[c]Laboratoire Jean-Perrin, Sorbonne Université, CNRS UMR 8237, 4 Place Jussieu, 75005 Paris, France

*Corresponding author: M. Ghomi, Tel: +33-1-48388928, E-mail: mahmoud.ghomi@univ-paris13.fr

ABSTRACT

During the last two decades, numerous observed data obtained by various physical techniques, also supported by molecular modeling approaches, have highlighted the structuring features of tripeptides, as well as their aggregation properties. Herein, we focus on the structural dynamics of four trimers, *i.e.*, Gly-Gly-Gly, Gly-Ala-Gly, Ala-Ala-Ala and Ala-Phe-Ala, in an aqueous environment. Density functional theory calculations (DFT) were carried out to assess the stability of four types of secondary structures, *i.e.*, β-strand, polyproline-II (pP-II), α-helix and γ-turn, of which the formation had been described in these tripeptides. Both implicit and explicit hydration effects were analyzed on the conformational and energetic features of trimers. It has been shown that the use of M062X functional (versus B3LYP) improve the stability of intramolecular H-bonds, especially in inverse γ-turn structures, as well as the energetic and conformational equilibrium in all tripeptides. Explicit hydration reflected by the presence of five water molecules around the backbone polar sites (NH_3^+, N-H, C=O and NH_2) considerably changes the conformational landscapes of the trimers. Characteristic intramolecular and intermolecular interactions evidenced by the calculations, were emphasized.

Keywords: Tripeptides; Conformational equilibrium; Extended chain; β-strand; γ-turn; Polyproline-II; α-helix; Density functional theory calculations

1. Introduction

Short size peptides are recognized as efficient bioactive [1-4], functional [5-7] and imaging agents [8] in biology and medicine. They are also considered as promising organic compounds to be used in bioinspired innovating materials [9,10]. In this framework, the aggregation properties of the short peptides in forming highly ordered self assemblies should be emphasized [11-14]. For instance, (i) the therapeutic octapeptide lanreotide (BIM 23014), a synthetic cyclic analogue of the natural hormone somatostatin, has shown its ability to form dimers, ribbons, nanotubes and liquide crystalline hexagonal phases upon increasing concentration [15-17]; (ii) controlled morphology of the self assembled amyloid β-based heptapeptide (Ala-Ala-Lys-Leu-Val-Phe-Phe) was studied in relation with its strong conductive properties [9]. The presence of aromatic residues within the short peptides was primarily believed to be the main factor in facilitating intermolecular associations through the so-called aromatic-aromatic (π-π) interactions. This fact has been nicely pointed out in a series of investigations showing the gradual auto-association followed by oligomerization of aromatic dipeptides, Phe-Phe and Phe-Trp [10], giving rise to quantum dots and semiconductive superstructures, also characterized by interesting absorption and photoluminescent features. Further studies on the coassemblies of aromatic dimer (Phe-Phe) and trimer (Phe-Phe-Phe) revealed various types of nanostructures appearing upon variation of their molar ratios [18]. Nevertheless, more recent observations highlighted that aromatic residues should not be considered as a prerequisite for initiating aggregation and nanostructures in short peptides. The exceptional case was the tripeptide Gly-Ala-Gly that forms long crystalline fibrils, and eventually hydrogels [19,20]. The above mentioned observations confirm the structuring trends, and the capability of short peptides to form intra- and intermolecular H-bonds, rendering possible the formation of nanostructures initiated by aggregation.

Several reports appeared in the last years were devoted to the secondary structural features of short peptides, such as di- and tripeptides. To cite just a few characteristic examples, we can emphasize (i) the in vacuum theoretical studies on the conformers adopted by TDA (acetylamino-L-tyrosyl-*N*-methylamide) [21]; (ii) the infrared hole burning and theoretical calculations on the classic and inverse γ-turn structures in a single proline with a NHMe (Me: methyl) and a benzyloxycarbonyl (abbreviated as Z) groups at its C^{ter} and N^{ter} sides, respectively [22]; (iii) a similar work as the preceding one but on the dipeptide, Z-Aib-Pro-NHMe (Aib: aminoisobutyryl) [23]; (iii) β-sheet and γ-turn conformations detected in the gas phase laser-desorbed jet-cooled of short sequences such as Ac–Phe–NHMe [24], Ac–Phe-Xxx-NH_2 (where Xxx=Gly, Ala, Val, Pro) [25], and Ac–Phe-Xxx-NH_2 (where Xxx=Aib, L-Ala, D-Ala) (Ac: acetyl) [26]; (iv) the theoretical investigation for exploring γ-turn in Ala repeats with the generic sequence Ac-Ala_n-NH_2 (n=2–4) [27]; and finally (v) the conformational preferences of short aromatic-capped glutamine containing molecular models studied under jet-cooled conditions [28]. Meanwhile, other approaches were being developed for the solution structural analysis of tripeptides [29-38], which are in fact based on the coupling between the characteristic vibrational motions arising from the two adjacent amide bonds [30-32]. Especially, a phenomenological perturbative theory was suggested [32,33] upon consideration of the so-called amide I vibrations, in which the coupling energy between the in-phase and out-of-phase motions the two carbonyl (C=O) bond-stretches was correlated to the difference between their observed wavenumbers. It was further shown that this methodology can lead to the assessment of the backbone geometrical parameters, such as (θ), the angle between the amide planes, as well as a characteristic pair of (Φ,ψ) angles, presumably assignable to the middle residue of a tripeptide. Further application of this approach to Ala-Ala-Ala and Gly-Gly-Gly has shown that both compounds are structured with some measurable differences from one to another [32,33]. Application of this approach

to the tripeptides with ionisable side chains (*i.e.*, Asp-Asp-Asp, Glu-Glu-Glu and Lys-Lys-Lys), revealed the coexistence of extended chains with those not belonging to the β-sheet region of Ramachandran plot [34,35]. More recent data obtained from the generic sequences Gly-Xxx-Gly (where Xxx=Ala, Val, Phe, Leu, Ser, Glu, Lys, Met) allowed exploration of polyproline-II (pP-II), β-strand, helical and γ-turn structures [36], as well as β-strand and pP-II in Ala-Phe-Ala [37] and Gly-Xxx-Gly (Xxx=Ile, Arg, Tyr) [38]. Other data provided by the combined use of CD, FT-IR and NMR experiments were consistent with the predominance of inverse γ-turn structure, coexisting with β-strand in the solution samples of Ala-Phe-Ala [39].

As a whole, the mentioned structural data obtained both in gas and solution states have confirmed the possible formation of secondary structures, such as β-strand, pP-II, α-helix and γ-turn in tripeptides. Herein, our objective was to assess the relative stability of these structures by considering both implicit and explicit hydration effects. Density functional theory (DFT) calculations by means of two different functionals (B3LYP and M062X) were carried out on four trimers, *i.e.*, Gly-Gly-Gly, Gly-Ala-Gly, Ala-Ala-Ala and Ala-Phe-Ala, selected for their increasing structural complexity, and availability of observed conformational data in aqueous solution.

2. Methods

2.1. *Tripeptides and their chemical composition*

The cationic species analyzed in this work were NH_3^+-Gly-Gly-Gly-$CONH_2$, NH_3^+-Gly-Ala-Gly-$CONH_2$, NH_3^+-Ala-Ala-Ala-$CONH_2$ and NH_3^+-Ala-Phe-Ala-$CONH_2$ (Fig. 1). All four compounds have the same backbone terminated by an amine and an amide at their N^{ter} and C^{ter} sides, respectively. Taking into account the high pK_a value corresponding to the amine group deprotonation, the backbone of all peptides keeps a cationic form

($NH_3^+/CONH_2$) within a wide pH interval (pH<10.5). For the sake of brevity, these four sequences are hereafter referred to as GGG, GAG, AAA, and AFA, respectively.

The choice of an amide group instead of a routinely used acid group is basically for avoiding the formation of folded structures induced by attractive electrostatic interactions between zwitterionic (NH_3^+/COO^-) end groups in an aqueous media [40]. It should be noted that a number of neurohypophyseal hormones, such as vasopressin and oxytocin, have an amide group at their C^{ter} side [41-44].

2.2. *Backbone and side chain rotamers*

As shown in Fig. 1, the backbone conformation of the considered tripeptides can be defined by seven torsion angles (ψ_1, ω_1, Φ_2, ψ_2, ω_2, Φ_3, ψ_3) around its successive bonds from N^{ter} to C^{ter} side [45], where the subscripts recall the residue numbers. Among these conformational angles, ω remains close to 180°, and the values assigned to the (Φ,ψ) angles depend on the backbone secondary structure. Limiting our analysis to β-strand, pP-II, γ-turn and α-helix secondary structures, the initial rotamers were constructed by using the mean values (Φ,ψ)= (-135°,+135°) for β-strand, (Φ,ψ)=(-75°,+150°) for pP-II, and (Φ,ψ)=(-60°,-45°) for α-helix. Two types of γ-turn, referred to as classic and inverse γ-turn [46,47], were considered, for which the (Φ_2,ψ_2) mean values were (+75°,-65°) and (-75°,+65°), respectively. In these folds, the (Φ,ψ) angles assigned to the other two residues were those relative to a β-strand. As a result, five initial conformers were constructed considered in GGG, GAG and AAA. In AFA, a higher conformational diversity exists thanks to the middle residue (F_2). Two additional torsion angles, namely (χ_1,χ_2), defined around the two successive side chain bonds (Fig.1), are required to account for the conformational flexibility of the Phe side chain [45], along which, C_α and C_β are of sp^3 type. Therefore, three privileged orientations, referred to as gauche$^+$ (or g^+) (60°±60°), gauche$^-$ (or g^-) and

(-60°±60°), and trans (or t) (180°±60°), can be *a priori* assigned to the torsion angle χ_1=Φ(N-C_α-C_β-C_γ). The initial values assigned to χ_1 were +60°, -60° and 180° corresponding to its g^+, g^- and t orientations, respectively. For χ_2=Φ(C_α-C_β-C_γ-$C_{\delta 1}$), we should naturally consider the rotation around the C_β-C_γ bond (Fig. 1), where C_γ is of sp^2 type. In this situation, the privileged orientations are thus g^+ (90°±90°) and g^- (-90°±90°) [48,49]. Due to the symmetry of the phenyl group, these two possible χ_2 values are equivalent, and can be noted by the unique notation $g^\pm$. As a consequence, two torsion angles with opposite signs (namely χ_2' and χ_2'', where (χ_2'-χ_2'') = ±180°) were assigned to each orientation. As a consequence, three distinct side chain orientations, *i.e.*, $g^+g^\pm$, $g^-g^\pm$ and $tg^\pm$, were taken into consideration for defining the Phe side chain. The initial value assigned to χ_2 was 90°. Considering the five aforementioned backbone conformations, and the three possible side chain orientations, the total number of initial conformers in AFA was 5x3=15.

2.3. *Geometry optimization*

The initial conformers of the four tripeptides (see Section 2.2 for details) were submitted to full geometry optimization by means of density functional theory (DFT) [50] calculations. Hybrid functional B3LYP [51,52] and M062X [53], along with polarized triple-zeta Gaussian atomic basis sets 6-311++G(d,p), were used in the present quantum chemical calculations. Hydration effects were considered by two complementary models: (i) a purely implicit model that consists in placing the solute in a polarizable continuum medium (PCM) [54,55], of which the relative permittivity was supposed to be that of water (ε_r=78.39); (ii) a mixture of implicit and explicit hydration models that considers a conformer interacting with five explicit water molecules embedded in the aforementioned continuum. Geometry optimization on each conformer was followed by harmonic vibrational calculations. The absence of any imaginary frequency confirmed the correspondence of an optimized geometry to a local energy

minimum. The energy order of the optimized geometries was based on their total energy (E_{tot}), which is the sum of electronic energy (E_e) and free energy correction ($E_{tot}=E_e$+free energy correction). Each optimized conformer discussed in this report is characterized by its relative energy (ΔE) as compared to that of the lowest energy conformer, for which ΔE is set to zero. All quantum mechanical calculations were performed with the Gaussian09 package [56].

3. Results and discussion

3.1. *Classification of optimized conformers*

Each optimized conformer has been assigned to a secondary structure on the basis of its (Φ_2,ψ_2) angles. We use here "extended chain" for describing a stretched/extended backbone with anti backbone torsion angles, even though in some cases the (Φ_2,ψ_2) couple adopts the values close to those routinely assigned to a β-strand. Classic and inverse γ-turn structures are all characterized by a closing H-bond between the backbone C=O (first residue) and N-H (third residue). A "helix" structure, issued from a conformer having initially an α-helix structure is characterized by a closing H-bond between the backbone C=O (first residue) and one of the hydrogen atoms of the C^{ter} amide group. This H-bond plays somehow the role of the so-called i→i+4 H-bond found in an α-helix. However, because of the lack of the fourth residue in a tripeptide, this type of structures was herein referred to as helix (instead of α-helix).

3.2. *B3LYP versus M062X functional. Deficiencies and advantages*

In the course of geometry optimization by means of B3LYP functional some surprising results appeared. For instance (i) in continuum, while the inverse γ-turn structure was stable in GGG, GAG and AAA (*i.e.*, keeping its characteristic torsion angles and closing H-bond), it

became unstable in AFA when the second residue (F_2) was in a $tg^{\pm}$ orientation. In fact, the latter initial conformer was transformed into an extended chain upon geometry optimization. Thus, it would have been possible to conclude that the $tg^{\pm}$ orientation destabilizes an inverse γ-turn because of the particular interactions occurring between the Phe side chain and the peptide backbone; (ii) in the presence of explicit water molecules, only GGG was shown to stabilize an inverse γ-turn. This could also bring us to the conclusion that the insertion of an Ala or a Phe residue in a tripeptide renders unstable an inverse γ-turn. In contrast, the calculated data obtained by means of M062X functional revealed the stability of an inverse γ-turn in all four peptides either in continuum or in the presence of explicit hydration. Furthermore, the analysis of the whole calculated data showed an irregular dispersion of the conformers optimized by means of B3LYP functional, not compatible with the existing observed conformational data. M062X functional improved the agreement between calculated and observed data (see Section 3.5 for details). It is worth emphasizing that previous investigations have reported on the superiority of M062X functional in the DFT calculations on the interactions of cisplatin (a widely used anticancer drug) with a carbon nanohorn [57] or a single wall carbon nanotube [58]. It has been shown that the use of M062X (versus B3LYP) provides better data concerning intermolecular interactions, energy order, and NMR chemical shifts.

Taking into account the above mentioned facts, we have chosen to limit our discussion to the calculated data obtained with the use of M062X functional. For the sake of brevity, only the graphical representations of the optimized structures, together with their relative energies, are displayed in Figs. 2-9. Other details relative to the backbone and side chain conformational angles are reported in Tables A1-A4 (Appendix A).

3.3. *Conformational and energetic landscapes in a polarisable continuum*

The optimized conformers of GGG, which is the structurally simplest and the most flexible analyzed tripeptide, are displayed in Fig. 2A-E. The lowest energy conformer (ΔE=0) is an extended chain issued from the optimization of a β-strand. The absolute values of the backbone torsion angles are all close to 180° (Table A1, Appendix A), giving a planar shape to this structure (Fig. 2A). It can be deduced that a conventional β-strand cannot be stabilized in GGG embedded in continuum. This result corroborates the previous DFT calculations on other G repeats placed in vacuum [59]. The peptides Ac-$(Gly)_n$-COOH (where n=3-5) show all a planar backbone whatever their initial conformation (PG-I or PG-II) [60]. Along the energy scale, helix (Fig. 2B), pP-II (Fig. 2C), and γ-turn (Fig. 2D,E) are located just above the lowest energy conformer. The highest relative energy (ΔE=+2.37 kcal/mol) is assigned to a classic γ-turn (Fig. 2E). In GAG (Fig. 3), helix becomes the lowest energy conformer (Fig. 3A). However, extended chain and pP-II are separated from helix by a quite small amount of energy (<1 kcal/mol) (Fig. 3B,C). As in the case of GGG, γ-turn structures are characterized by the highest relative energies (Fig. 3D,E). In AAA, extended chain, inverse γ-turn, helix and pP-II (Fig. 4A-D) are separated one from another by a small amount of energy. In this case, classic γ-turn is also characterized by the highest relative energy (ΔE=+2.83 kcal/mol) (Fig. 4E). At last, the optimized conformers of AFA are presented in Fig. 5A-O, showing the effect of both the backbone secondary structure and the Phe side chain orientation on their relative energies. One can emphasize that extended chains are all located among the lowest energy conformers (Fig. 5A,B,E), and the highest relative energies are associated to classic γ-turn structures (Fig. 5K,M,O).

3.4. *Conformational and energetic landscapes upon explicit hydration*

In the first step of this study, we attempted to find a homogeneous and transferable hydration environment around the common backbone of the considered peptides As known, water is as a polar molecule acting both as an H-bond donor and acceptor, which can naturally interact with the backbone C=O, N-H, NH_2 and NH_3^+ groups (Fig. 1). Taking into account the protocols described in the previous reports on the privileged hydration sites of amino acids [40,61], our aim was to find a minimal number of water molecules allowing achievement of an optimal interaction with all the aforementioned polar sites. As a consequence, two water molecules were used for hydrating the two terminal NH_3^+ and NH_2 groups, and three others for interacting each one with the neighbouring C=O and N-H groups. The conformational angles of the explicitly hydrated conformers are reported in Tables A1, A2 and A4 (Appendix A).

The five different optimized clusters of GGG+5H_2O, GAG+5H_2O, AAA+5H_2O, as well as the fifteen clusters of AFA+5H_2O are displayed in Figs. 6-9, respectively. The most surprising effect appearing upon explicit hydration is that helical conformer becomes the most stable one in GGG, GAG and AAA ($\Delta E=0$), separated from pP-II by an energy amount varying between 0.26 and 1.49 kcal/mol (Figs. 6-8). Another interesting effect is that the initial conformer with a β-strand structure is transformed into a pP-II type conformation in GGG and AAA (Fig. 6C, Fig. 8D). In AFA, pP-II conformers with different Phe side chain orientations were found to be the most stable ones (Fig. 9A-C), followed by helical conformers and extended chains (Fig.9D-G).

3.5. *Assessment of populations of different conformers*

To overview the changes occurring in the energy and conformational landscapes of the tripeptides, the Boltzmann thermal weights of the five considered secondary structures were

calculated by means of their relative energies (ΔE) (Figs. 6-9, Tables A1-A4, Appendix A). The obtained data are displayed in Fig. 10. In GGG and AFA embedded in continuum, more than half of the conformers correspond to extended chains (Fig. 10A,D), whereas helical conformers dominate in GAG. In contrast, in AAA (Fig. 10C), a mixture of four conformers (extended chain, inverse γ-turn, helix and pP-II) is predicted. The situation substantially changes upon explicit hydration (Fig. 10E-H), where helix and pP-II structures become dominant. While more than 50% of conformers are helical in GGG and GAG (Fig. 10E,F), this high proportion is reached for pP-II conformers in AFA (Fig. 10H). As in the case of the calculations in continuum a mixture of three types of conformations (helix, pP-II and inverse γ-turn) is predicted in AAA (Fig. 10G).

The calculated populations obtained either in continuum or in the presence of explicit water molecules (Fig. 10) allow us to bring a qualitative interpretation to the previous observations on the analyzed trimers [32,33,36,37]. In agreement with the conclusions derived previously the calculations upon implicit (Fig. 10A,C) and explicit (Fig. 10E,G) hydration show that the homotrimers GGG and AAA present different populations. On the other hand, the simultaneous presence of several types of secondary structures is confirmed by the calculated data in GAG (Fig. 10B,D) and AFA (Fig. 10F,H).

3.6. *Focus on intermolecular and intermolecular interactions*

The present calculated data permitted appreciation of the intramolecular and intermolecular interactions in tripetides. For instance, the length of the characteristic intramolecular H-bond is estimated around 2.08 Å in helix, between 2.04 and 2.14 Å in classic γ-turn, and between 2.14 and 2.20 Å in inverse γ-turn structures (Figs. 2-4). As far as the intermolecular H-bonds are concerned, very short H-bonds (1.72-1.75 Å) were revealed between the positively charged amine group (NH_3^+) and a surrounding water molecule (W).

Longer H-bonds (1.78-1.88 Å) characterize the C=O...H_w interactions. Finally, the N-H…O_W type interactions were found to be the longest intermolecular H-bonds (1.85-2.00 Å) (Figs. 6-8).

Other types of intermolecular interactions are also to be emphasized. The first type is the so-called H_W…π interactions occurring between the water molecules and the phenyl ring (in AFA) (Fig. 11A). This interaction was first reported in benzene [62], and further emphasized in other organic molecules [63]. Recently, H_W…π interactions were extensively analyzed in aromatic amino acids (Phe, Tyr, Trp, His) [64]. Their binding energy was estimated to be ~2 kcal/mol, *i.e.*, lower than that characterizing a traditional planar H-bond [61]. The second type of interactions is referred to as aliphatic-aromatic appearing between adjacent Ala and Phe residues, which is favored by certain backbone conformations and aromatic side chain orientations (Fig. 11B-D).

4. Concluding remarks

The main objective of this paper was to bring insight into the structuring features of the tripeptides in aqueoeus environment. Stability and energy order of the secondary structures, such as β-strands, pP-II, γ-turn and helix, of which the presence was confirmed in aqueous samples, was assessed by DFT calculations. Four tripeptides (GGG, GAG, AAA and AFA) were analyzed by means of B3LYP and M062X functionals. In this framework, the superiority of M062X functional concerning the stability of intramolecular H-bonds, especially in inverse γ-turn structures, was shown. This can be explained by a better correction of the dispersion interactions by M062X functional [58]. Although a minimal number (five) of hydrating water molecules interacting with the backbone privileged hydration sites was considered, the explicit hydration was shown to drastically change the conformational equilibrium in tripeptides. While extended chain and helix appear to be the

major conformers in a polarizable continuum, the populations of pP-II and helical conformers dominate in the presence of water molecules. In all peptides, the highest relative energies were attributed to classic γ-turn structures. The calculated data confirm two different conformational landscapes for the homotrimers GGG and AAA, as suggested by the previously reported experimental data [32,33]; they also confirm the presence of several types of secondary structures in GAG and AFA [36,37].

The present investigation leads us to conclude that M062X/6-311++G(d,p) level can be confidently used in further theoretical calculations on the structural and energetic analyses on short peptides in aqueous environment. Certainly, comparison should also be made between M062X and other functionals, such as ωB97X-D that provided highly reliable calculated data in a large number of organic molecules [64]

Acknowledgements

The theoretical calculations described here were granted access to the HPC resources of CINES/IDRIS under the allocations A0060805065 made by Grand Equipement National de Calcul Intensif (GENCI).

References

[1] A. Heinz, Elastases and elastokines: elastin degradation and its significance in health and disease, Crit. Rev. Biochem. Mol. Biol. 55 (2020) 252-273.

[2] J. Zhou, M. Chen, S. Wu, X. Liao, J. Wang, Q. Wu,, M. Zhuang, Y. Ding, A review on mushroom-derived bioactive peptides: Preparation and biological activities, Food Res. Int. 134 (2020) 109230.

[3] C. M. Scheidler, L. M. Kick, S. Schneider, Ribosomal Peptides and Small Proteins on the Rise, Chembiochem. 20 (2019) 1479-1486.

[4] M. Hashemzehi, F. Beheshti, S. Hassanian, G. A. Ferns, M. Khazaei, Therapeutic potential of renin angiotensin system inhibitors in cancer cells metastasis, Avan A. Pathol. Res. Pract. 216 (2020) 153010.

[5] H. van der Weide, U. Cossío, R. Gracia, Y. M. Te Welscher, M. T. Ten Kate, A. van der Meijden, M. Marradi, J. A. S. Ritsema, D. M. C. Vermeulen-de Jongh, G. Storm, W. H. F. Goessens, I. Loinaz, C. F. van Nostrum, J. Llop, J. P. Hays, I. A. J. M. Bakker-Woudenberg, Therapeutic efficacy of novel antimicrobial peptide AA139-nanomedicines in a multidrug-resistant Klebsiella pneumoniae pneumonia-septicemia model in rats, Antimicrob. Agents Chemother. (2020) doi: 10.1128/AAC.00517-20.

[6] L. F. Awad, M. S. Ayoup, Fluorinated phenylalanines: synthesis and pharmaceutical applications, Beilstein J. Org. Chem. 16 (2020) 1022-1050.

[7] S. Wen, W. Wang, R. Liu, P. He, Amylase-Protected Ag Nanodots for in vivo Fluorescence Imaging and Photodynamic Therapy of Tumors, Int. J. Nanomedicine 15 (2020) 3405–3414.

[8] H. Li, L. Yuan, Y. Long, H. Fang, M. Li, Q. Liu, X. Xia, C, Qin, Y. Zhang, X. Lan , Y. Gai, Synthesis and preclinical evaluation of a 68Ga-radiolabeled peptide targeting very late antigen-3 for PET imaging of pancreatic cancer, Mol. Pharm. (2020), doi: 10.1021/acs.molpharmaceut.0c00416.

[9] M. Amit, G. Cheng, I. W. Hamley, N. Ashkenasy, Conductance of amyloid β based peptide filaments: Structure-function relations, Soft Matter 8 (2012) 8690–8696.

[10] K. Tao, P. Makam, R. Aizen, E. Gazit, Self-assembling peptide semiconductors, Science 358 (2017) eaam9756.

[11] J. Wang , J. Jia , Y. Wang , Q. Xing, X. Peng , W. Qi , R. Su , Z. He, Protamine-induced Condensation of Peptide Nanofilaments Into Twisted Bundles With Controlled Helical Geometry, J. Pept. Sci. 25 (2019) e3176.

[12] Y. Wang, Y. Feng, X. Yang, J. Wang, W. Qi, X. Yang, X. Liu, Q. Xing, R. Su, Z. He. Hexagonally Ordered Arrays of α-Helical Bundles Formed from Peptide-Dendron Hybrids, Soft Matter 15 (2019) 4818-4826.

[13] S. Bera, E. Gazit, Self-assembly of Functional Nanostructures by Short Helical Peptide Building Blocks, Protein Pept. Lett. 26 (2019) 88-97.

[14] P. Makam, E. Gazit, Minimalistic peptide supramolecular co-assembly: expanding the conformational space for nanPolyamine-induced, chiral expression from liquid crystalline peptide nanofilaments to long-range ordered nanohelices, Chem. Soc. Rev. 47 (2018) 3406-3420.

[15] Tarabout, S. Roux, F. Gobeaux, N. Fay, E. Pouget, C. Meriadec, M. Ligeti, D. Thomas, M. IJsselstijn, F. Besselievre, D. A. Buisson, J. M. Verbavatz, M. Petitjean, C. Valéry, L. Perrin, B. Rousseau, F. Artzner, M. Paternostre, J. C. Cintrat,, Control of peptide nanotube diameter by chemical modifications of an aromatic residue involved in a single close contact, Proc. Natl. Acad. Sci. U. S. A. 108 (2011) 7679–7684.

[16] C. Valéry, E. Pouget, A. Pandit, J. M. Verbavatz, L. Bordes, I. Boisdé, R. Cherif-Cheikh, F. Artzner, M. Paternostre, Molecular Origin of the Self-Assembly of Lanreotide into Nanotubes: A Mutational Approach, Biophys. J. 94 (2008) 1782–1795.

[17] C. Valéry, M. Paternostre, B. Robert, T. Gulik-Krzywicki, T. Narayanan, J. C. Dedieu, G. Keller, M. L. Torres, R. Cherif-Cheikh, P. Calvo, F. Artzner, Biomimetic organization: Octapeptide self-assembly into nanotubes of viral capsid-like dimension, Proc. Natl. Acad. Sci. U. S. A. 100 (2003) 10258–10262.

[18] C. Guo , Z. A. Arnon, R. Qi, Q. Zhang , L. Adler-Abramovich, E. Gazit, G. Wei, Expanding the Nanoarchitectural Diversity Through Aromatic Di- And Tri-Peptide Coassembly: Nanostructures and Molecular Mechanisms, ACS Nano 10 (2016) 8316–8324.

[19] N. V. Ilawe, R. Schweitzer-Stenner, D. DiGuiseppi, B. M. Wong, Is a cross-β-sheet structure of low molecular weight peptides necessary for the formation of fibrils and peptide hydrogels?, Phys. Chem. Chem. Phys. 20 (2018) 18158-18168.

[20] D. M. DiGuiseppi, L. Thursch , N. J. Alvarez, R. Schweitzer-Stenner, Exploring the gel phase of cationic glycylalanylglycine in ethanol/water. II. Spectroscopic, kinetic and thermodynamic studies, J. Coll. Int. Sci. 573 (2020) 123–134.

[21] E. Langella, N. Rega, R. Importa, O. Crescenzi, V. Barone, Conformational analysis of the tyrosine dipeptide analogue in the gas phase and in aqueous solution by a density functional/continuum solvent model, J. Comput. Chem. 23 (2002) 650–661.

[22] I. Compagnon, J. Oomens, J. Bakker, G. Meijer, G. von Helden, Vibrational spectroscopy of a non-aromatic amino acid-based model peptide: identification of the γ-turn motif of the peptide backbone, Phys. Chem. Chem. Phys. 7 (2005) 13-15.

[23] I. Compagnon, J. Oomens, G. Meijer, G. von Helden, Mid-Infrared Spectroscopy of Protected Peptides in the Gas Phase: A Probe of the Backbone Conformation, J. Am. Chem. Soc. 128 (2006) 3592-3597.

[24] M. Gerhards, C. Unterberg, A. Gerlach, A. Jansen, β-sheet model systems in the gas phase: Structures and vibrations of Ac–Phe–NHMe and its dimer $(Ac–Phe–NHMe)_2$, Phys. Chem. Chem. Phys. 6 (2004) 2682-2690.

[25] W. Chin, F. Piuzzi F, J. P. Dognon, I. Dimicoli, M. Mons, Gas-phase models of γ-turns: effect of side-chain/backbone interactions investigated by IR/UV spectroscopy and quantum chemistry, J. Chem. Phys. 123 (2005) 084301.

[26] E. Gloaguen, F. Pagliarulo, V. Brenner, W. Chin, F. Piuzzi, B. Tardivel, M. Mons, Intramolecular recognition in a jet-cooled short peptide chain: γ-turn helicity probed by a neighbouring residue, Phys. Chem. Chem. Phys. 9 (2007) 4491–4497.

[27] G. Lanza, M. A. Chiacchio, Comprehensive and accurate ab initio energy surface of simple alanine peptides, Chem. Phys. Chem. 14 (2013) 3284-3293.

[28] P. S. Walsh, J. C. Dean, C. McBurney, H. Kang, S. H. Gellman, T. S. Zwier, Conformation-specific spectroscopy of capped glutamine-containing peptides: role of a single glutamine residue on peptide backbone preferences, Phys. Chem. Chem. Phys. 18 (2016) 11306-11322.

[29] H. Torii, M. Tasumi, Ab initio molecular orbital study of the amide I vibrational interactions between the peptide groups in di- and tripeptides and considerations on the conformation of the extended helix, J. Raman Spectrosc. 29 (1998) 81-86.

[30] S. Woutersen, P. Hamm, Structure determination of trialanine in water using polarization sensitive two-dimensional vibrational spectroscopy, J. Phys. Chem. B. 104 (2000) 11316-11320.

[31] S. Woutersen, P. Hamm, Isotope-edited two-dimensional vibrational spectroscopy of trialanine in aqueous solution, J. Chem. Phys. 114 (2001) 2727-2737.

[32] R. Schweitzer-Stenner, F. Eker, Q. Huang, K. Griebenow, Dihedral angles of trialanine in D_2O determined by combining FTIR and polarized visible Raman spectroscopy, J. Am. Chem. Soc. 123 (2001) 9628-9633.

[33] R. Schweitzer-Stenner, Dihedral angles of tripeptides in solution directly determined by polarized Raman and FTIR spectroscopy, Biophys. J. 83 (2002) 523–532.

[34] F. Eker, K. Griebenow, R. Schweitzer-Stenner, Stable conformations of tripeptides in aqueous solution studied by UV circular dichroism spectroscopy, J. Am. Chem. Soc. 125 (2003) 8178-8185.

[35] F. Eker, K. Griebenow, X. Cao, L. A. Nafie, R. Schweitzer-Stenner, Tripeptides with ionizable side chains adopt a perturbed polyproline II structure in water, Biochemistry 43 (2004) 613-621.

[36] A. Hagarman, T. J. Measey, D. Mathieu, H. Schwalbe, R. Schweitzer-Stenner, Intrinsic Propensities of amino acid residues in GxG peptides inferred from amide I′ band profiles and NMR scalar coupling constants, J. Am. Chem. Soc. 132 (2010) 540–551.

[37] S. Pizzanelli, C. Forte, S. Monti, G. Zandomeneghi, A. Hagarman,T. J. Measey, R. Schweitzer-Stenner, Conformations of phenylalanine in the tripeptides AFA and GFG probed by combining MD simulations with NMR, FTIR, polarized Raman, and VCD spectroscopy, J. Phys. Chem. B 114 (2010) 3965-3978.

[38] R. Schweitzer-Stenner, A. Hagarman, S. Toal, D. Mathieu, H. Schwalbe, Disorder and order in unfolded and disordered peptides and proteins: A view derived from tripeptide conformational analysis. I. Tripeptides with long and predominantly hydrophobic side chains, Proteins 81 (2013) 955–967.

[39] A. Motta , M. Reches, L. Pappalardo, G. Andreotti, E. Gazit, The Preferred Conformation of the Tripeptide Ala-Phe-Ala in Water Is an Inverse Gamma-Turn: Implications for Protein Folding and Drug Design, Biochemistry 44 (2005) 14170-14178.

[40] B. Hernández, F. Pflüger, M. Ghomi, Aspartate: An interesting model for analyzing dipole-ion and ion pair interactions through its oppositely charged amine and acid groups, J. Comput. Chem. 41 (2020) 1402-1410.

[41] Z. Grzonka, E. Gwizdała, F. Kasprzykowski, L. ŁaneKiewicz, Circular dichroism studies of some arginine-vasopressin analogues, Biophys. Chem. 31 (1988) 87-100.

[42] I. Fric, J. Hlavacek, T. W. Rockway, W. Y. Chan, V. J. Hruby, Effects of conformational constraint in 2- and 8-cycloleucine analogues of oxytocin and [1-penicillamine] oxytocin examined by circular dichroism and biosassay, J. Protein Chem. 9 (1990) 9-15.

[43] V.S. Ananthanarayanan, K. S. Brimble, Interaction of oxytocin with Ca^{2+}: I. CD and fluorescence spectral characterization and comparison with vasopressin, Biopolymers 40 (1996) 433-443.

[44] M. Pazderková, L. Bednárová, H. Dlouhá, M. Flegel, M. Lebl, J. Hlaváček, V. Setnička, M. Urbanová, S. Hynie, V. Klenerová, V. Baumruk, P. Maloň, Electronic and vibrational optical activity of several peptides related to neurohypophyseal hormones: Disulfide group conformation, Biopolymers 97 (2012) 923-932.

[45] G. E. Schulz, R. H. Schirmer, Principles of protein structure, Berlin: Springer-Verlag, 1979.

[46] R. Kishore, P. Balaram, Stabilization of γ-turn conformations in peptides by disulfide bridging, Biopolymers 24 (1985) 2041-2043.

[47] E. J. Milner-White, B. M. Ross, R. Ismail, K. Belhadj-Mostefa, R. Poet, One type of gamma-turn, rather than the other gives rise to chain-reversal in proteins, J. Mol. Biol. 204 (1988) 777–782.

[48] B. Hernández, F. Pflüger, A. Adenier, S. G. Kruglik, M. Ghomi, Vibrational analysis of amino acids and short peptides in hydrated media. VIII. Amino Acids with Aromatic Side Chains: L-Phenylalanine, L-Tyrosine, and L-Tryptophan, J. Phys. Chem. B 114 (2010) 15319–15330.

[49] B. Hernández, F. Pflüger, A. Adenier, S. G. Kruglik, M. Ghomi, Characteristic Raman lines of phenylalanine analyzed by a multiconformational approach, J. Raman Spectrosc. 44 (2013) 827-833.

[50] W. Kohn, L. J. Sham, Self-consistent equations including exchange and correlation effects, Phys. Rev. 140 (1965) A1133–A1138.

[51] C. Lee, W. Yang, R. G. Parr, Development of the Colle-Salvetti correlation-energy formula into a functional of the electron density, Phys. Rev. B: Condens. Matter Mater. Phys. 37 (1988) 785–789.

[52] A. D. Becke, Density-functional thermochemistry. III. The role of exact exchange, J. Chem. Phys. 98 (1993) 5648–5652.

[53] Y. Zhao, D. G. Truhlar, The M06 suite of density functional for main group thermochemistry, thermochemical kinetics, noncovalent interactions, excited states, and transition elements: two

new functionals and systematic testing of four M06-class functionals and 12 other functionals, Theor. Chem. Acc. 120 (2008) 215-341.

[54] V. Barone, M. Cossi, Quantum calculation of molecular energies and energy gradients in solution by a conductor solvent model, J. Phys. Chem. A 102 (1988) 1995–2001.

[55] M. Cossi, N. Rega, G. Scalmani and V. Barone, Energies, structures, and electronic properties of molecules in solution with the C-PCM solvation model, J. Comput. Chem. 24 (2003) 669–681.

[56] M. J. Frisch, G. W. Trucks, H. B. Schlegel, G. E. Scuseria, M. A. Robb, J. R. Cheeseman, G. Scalmani, V. Barone, B. Mennucci, G. A. Petersson, H. Nakatsuji, M. Caricato, X. Li, H. P. Hratchian, A. F. Izmaylov, J. Bloino, G. Zheng, J. L. Sonnenberg, M. Hada, M. Ehara, K. Toyota, R. Fukuda, J. Hasegawa, M. Ishida, T. Nakajima, Y. Honda, O. Kitao, H. Nakai, T. Vreven, J. A. Montgomery, Jr., J. E. Peralta, F. Ogliaro, M. Bearpark, J. J. Heyd, E. Brothers, K. N. Kudin, V. N. Staroverov, T. Keith, R. Kobayashi, J. Normand, K. Raghavachari, A. Rendell, J. C. Burant, S. S. Iyengar, J. Tomasi, M. Cossi, N. Rega, J. M. Millam, M. Klene, J. E. Knox, J. B. Cross, V. Bakken, C. Adamo, J. Jaramillo, R. Gomperts, R. E. Stratmann, O. Yazyev, A. J. Austin, R. Cammi, C. Pomelli, J. W. Ochterski, R. L. Martin, K. Morokuma, V. G. Zakrzewski, G. A. Voth, P. Salvador, J. J. Dannenberg, S. Dapprich, A. D. Daniels, O. Farkas, J. B. Foresman, J. V. Ortiz, J. Cioslowski, D. J. Fox, Gaussian 09, Revision D.01, Gaussian, Inc., Wallingford CT, 2013.

[57] L. A. De Souza, C.A.S. Nogueira, J. F. Lopes, H. F. Dos Santos, W. B. De Almeida, DFT study of cisplatin@carbon nanohorns complexes, J. Inorg. Biochem. 129 (2013) 71–83.

[58] L. A. De Souza, C. A.S. Nogueira, J. F. Lopes, H. F. Dos Santos, W. B. De Almeida, Theoretical Study of the Formation of Inclusion Complex between Cisplatin and Single-Wall Carbon Nanotube, J. Phys. Chem. C 119 (2015) 8394–8401.

[59] S. Bee, N. Choudhary, A. Gupta, P. Tandon, Molecular Structure and Vibrational Spectra of N-Acetylglycine Oligomers and Polyglycine I using DFT approach, Biopolymers 101 (2014) 795-813.

[60] S. Bykov, S. Asher, Raman studies of Solution Polyglycine Conformations, J. Phys. Chem. B 114 (2010) 6636–6641.

[61] B. Hernández, F. Pflüger, M. Dauchez, M. Ghomi, Privileged hydration sites in aromatic side chains: effect on conformational equilibrium, Phys. Chem. Chem. Phys. 19 (2017) 28684-28695.

[62] S. Suzuki, P. G. Green, R. E. Bumgarner, S. Dasgupta, W. A. Goddard III, G. A. Blake, Benzene forms hydrogen bonds with water, Science 257 (1992) 942–945.

[63] M. Mons, E. G. Robertson, J. P. Simons, Intra- and Intermolecular π-Type Hydrogen Bonding in Aryl Alcohols: UV and IR-UV Ion Dip Spectroscopy, J. Phys. Chem. A 104 (2000) 1430-1437.

[64] N. Dandu, L. Ward, R. S. Assary, P. C. Redfern, B. Narayanan, I. T. Foster, L. A. Curtiss, Quantum-Chemically Informed Machine Learning: Prediction of Energies of Organic Molecules with 10 to 14 Non-hydrogen Atoms, J. Phys. Chem. A 124 (2020) 5804−5811.

Figure captions

Fig. 1 Chemical composition and atomic nomenclatures of the backbone and side chain of the analyzed tripeptides.

Fig. 2 Graphical representation of the five optimized structures for the GGG cationic species embedded in a polarizable continuum.
From bottom to top the structures are presented in the increasing order of their relative energy (ΔE) as expressed in kcal/mol. Characteristic intramolecular H-bonds are drawn in broken green lines, of which the length (in Å) is displayed.

Fig. 3 Graphical representation of the five optimized structures for the GAG cationic species embedded in a polarizable continuum.
From bottom to top the structures are presented in the increasing order of their relative energy (ΔE) as expressed in kcal/mol. Characteristic intramolecular H-bonds are drawn in broken green lines, of which the length (in Å) is displayed. The sign (+) designates the location of the terminal NH_3^+ group.

Fig. 4 Graphical representation of the five optimized structures for the AAA cationic species embedded in a polarizable continuum.
From bottom to top the structures are presented in the increasing order of their relative energy (ΔE) as expressed in kcal/mol. Characteristic intramolecular H-bonds are drawn in broken green lines, of which the length (in Å) is displayed.

Fig. 5 Graphical representation of the fifteen optimized structures for the AFA cationic species embedded in a polarizable continuum.
From bottom to top the structures are presented in the increasing order of their relative energy (ΔE) as expressed in kcal/mol. $g^+g^\pm$, $g^-g^\pm$ and $tg^\pm$ notations recall the side chain orientation of the middle residue (see text for details). Characteristic intramolecular H-bonds are drawn in broken green lines, of which the length (in Å) is displayed.

Fig. 6 Graphical representation of the five optimized structures for the GGG+5H_2O clusters embedded in a polarizable continuum.
From bottom to top the structures are presented in the increasing order of their relative energy (ΔE) as expressed in kcal/mol. Characteristic intra- and intermolecular H-bonds are drawn in broken green lines, of which the length (in Å) is displayed.

Fig. 7 Graphical representation of the five optimized structures for the GAG+5H_2O clusters embedded in a polarizable continuum.
From bottom to top the structures are presented in the increasing order of their relative energy (ΔE) as expressed in kcal/mol. Characteristic intra- and intermolecular H-bonds are drawn in broken green lines, of which the length (in Å) is displayed.

Fig. 8 Graphical representation of the five optimized structures for the AAA+5H_2O clusters embedded in a polarizable continuum.
From bottom to top the structures are presented in the increasing order of their relative energy (ΔE) as expressed in kcal/mol. Characteristic intra- and intermolecular H-bonds are drawn in broken green lines, of which the length (in Å) is displayed.

Fig. 9 Graphical representation of the fifteen optimized structures for the AFA+5H_2O clusters embedded in a polarizable continuum.
From bottom to top the structures are presented in the increasing order of their relative energy (ΔE) as expressed in kcal/mol. For the sake of clarity, only the intramolecular H-bonds are drawn in broken green lines, of which the length (in Å) is displayed. The intermolecular H-bonds are very close to those found in AAA+5H_2O (Fig. 8).

Fig. 10 Histograms representing the normalized Boltzmann thermal weights for the five analyzed secondary structure.
Above each bar the value of the thermal weight as expressed in percent is reported. Only the weights ≥1% were displayed.

Fig. 11 Graphical representation intramolecular and intermolecular interactions evidenced by in AFA. (A) H_W... π interaction between the water molecule and the phenyl ring. (B-D) aliphatic-aromatic interactions between the adjacent Ala and Phe residues.
H-bonds are drawn in broken green lines, of which the length (in Å) is displayed. Backbone conformation and side chain orientation are also indicated below each case.

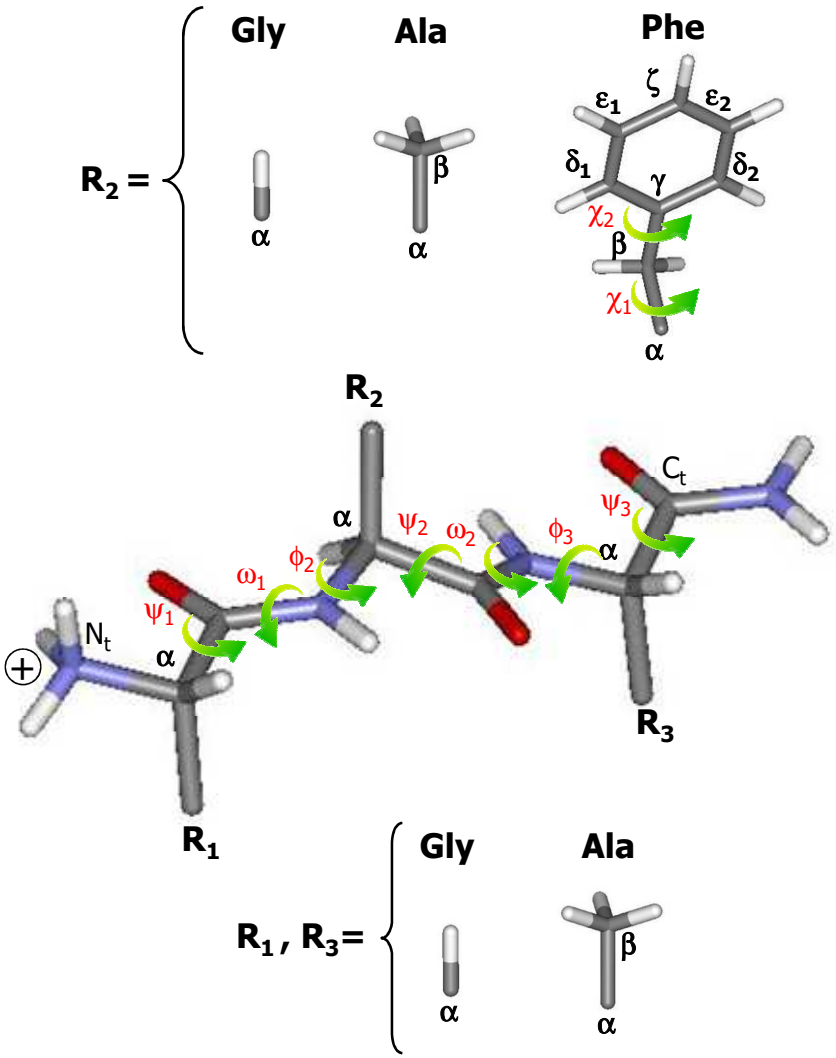

Fig. 1 Chemical composition and atomic nomenclatures of the backbone and side chain of the analyzed tripeptides.

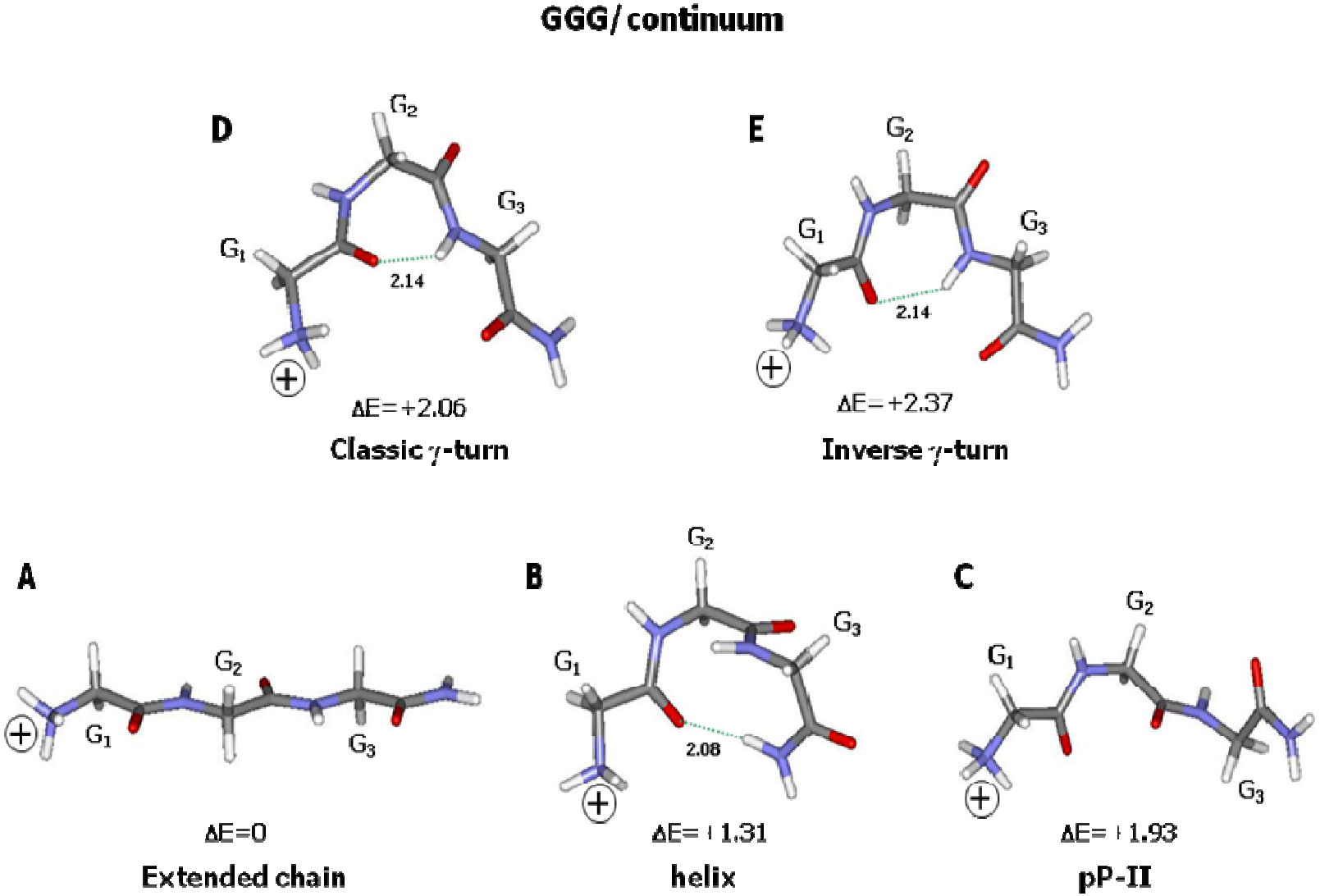

Fig. 2 Graphical representation of the five optimized structures for the GGG cationic species embedded in a polarizable continuum.

From bottom to top the structures are presented in the increasing order of their relative energy (ΔE) as expressed in kcal/mol. Characteristic sign (+) designates the location of the terminal NH_3^+ group.

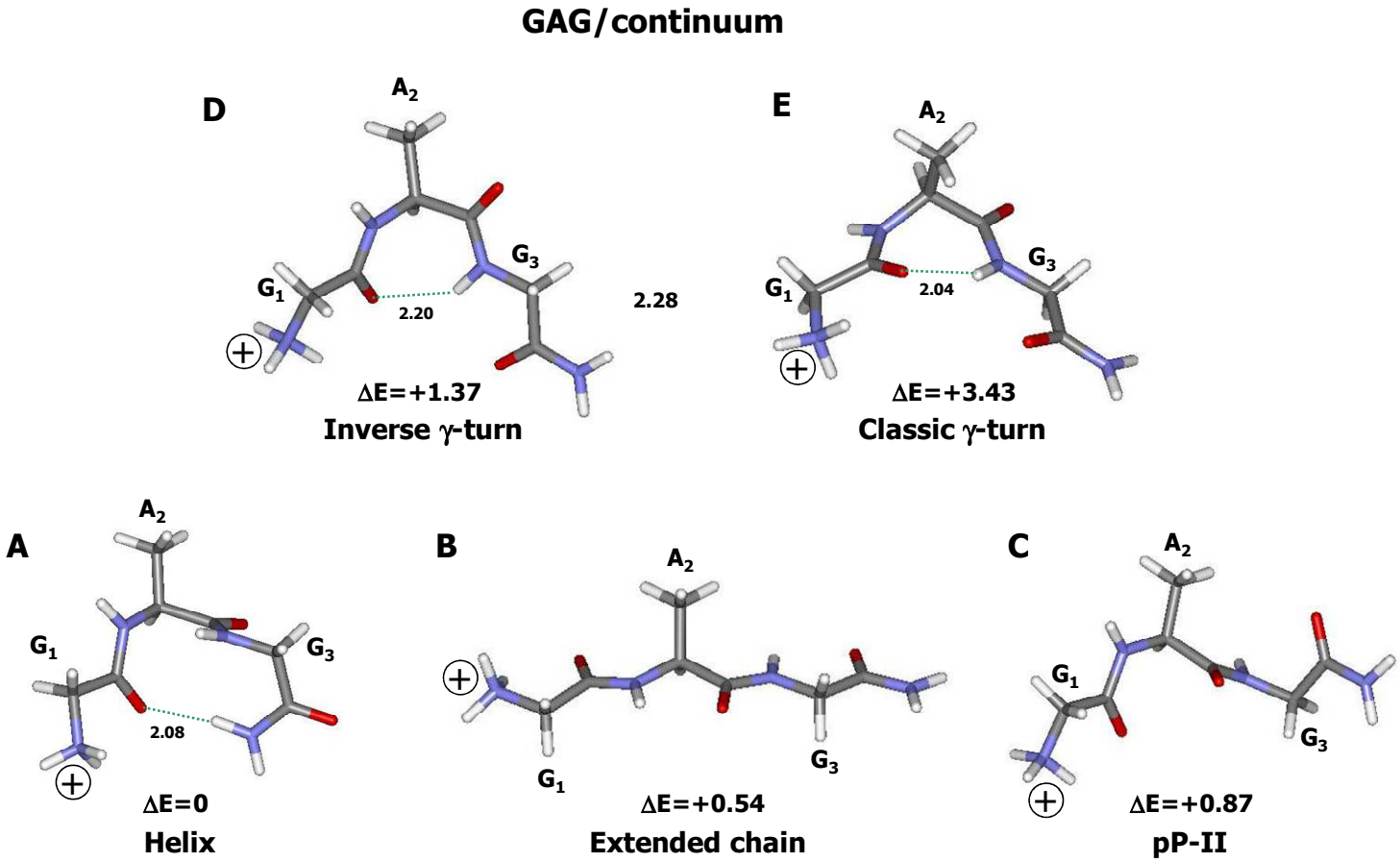

Fig. 3 Graphical representation of the five optimized structures for the GAG cationic species embedded in a polarizable continuum.

From bottom to top the structures are presented in the increasing order of their relative energy (ΔE) as expressed in kcal/mol. Characteristic intramolecular H-bonds are drawn in broken green lines, of which the length (in Å) is displayed.

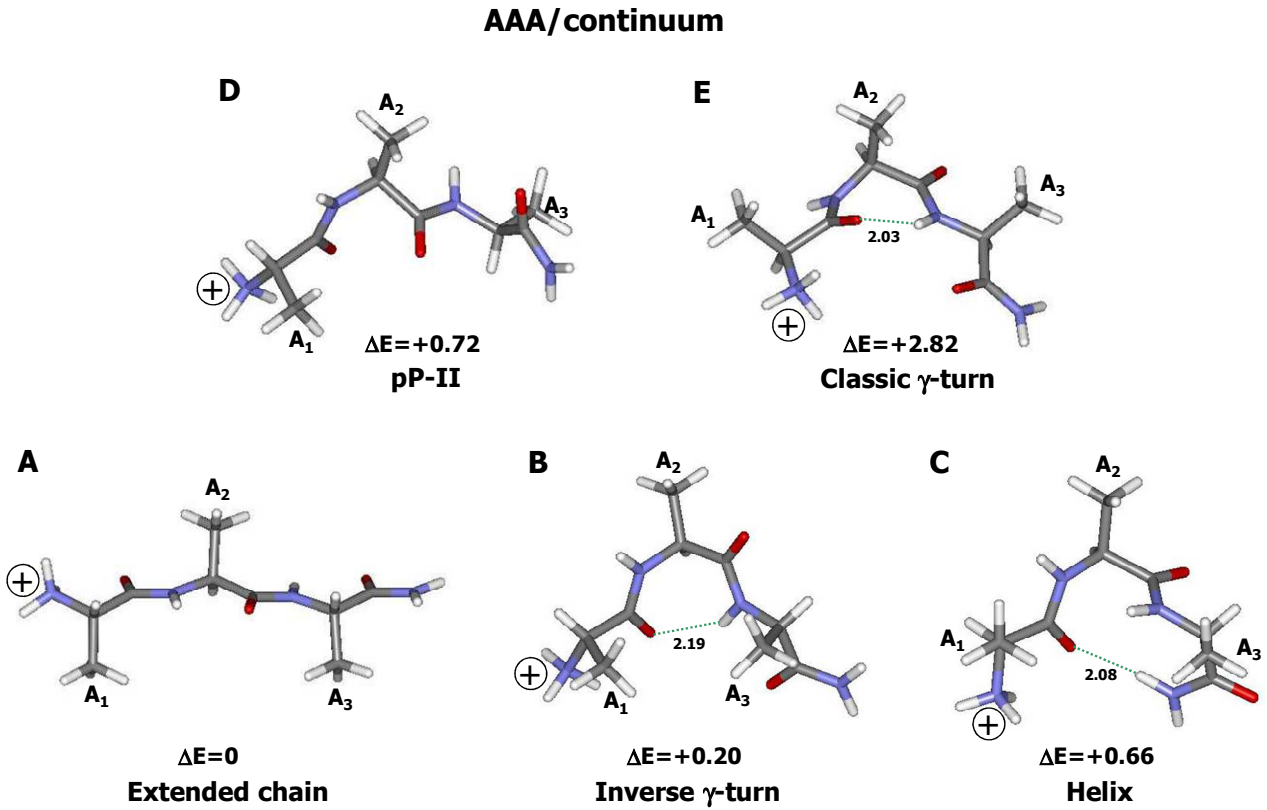

Fig. 4 Graphical representation of the five optimized structures for the AAA cationic species embedded in a polarizable continuum.

From bottom to top the structures are presented in the increasing order of their relative energy (ΔE) as expressed in kcal/mol. Characteristic intramolecular H-bonds are drawn in broken green lines, of which the length (in Å) is displayed.

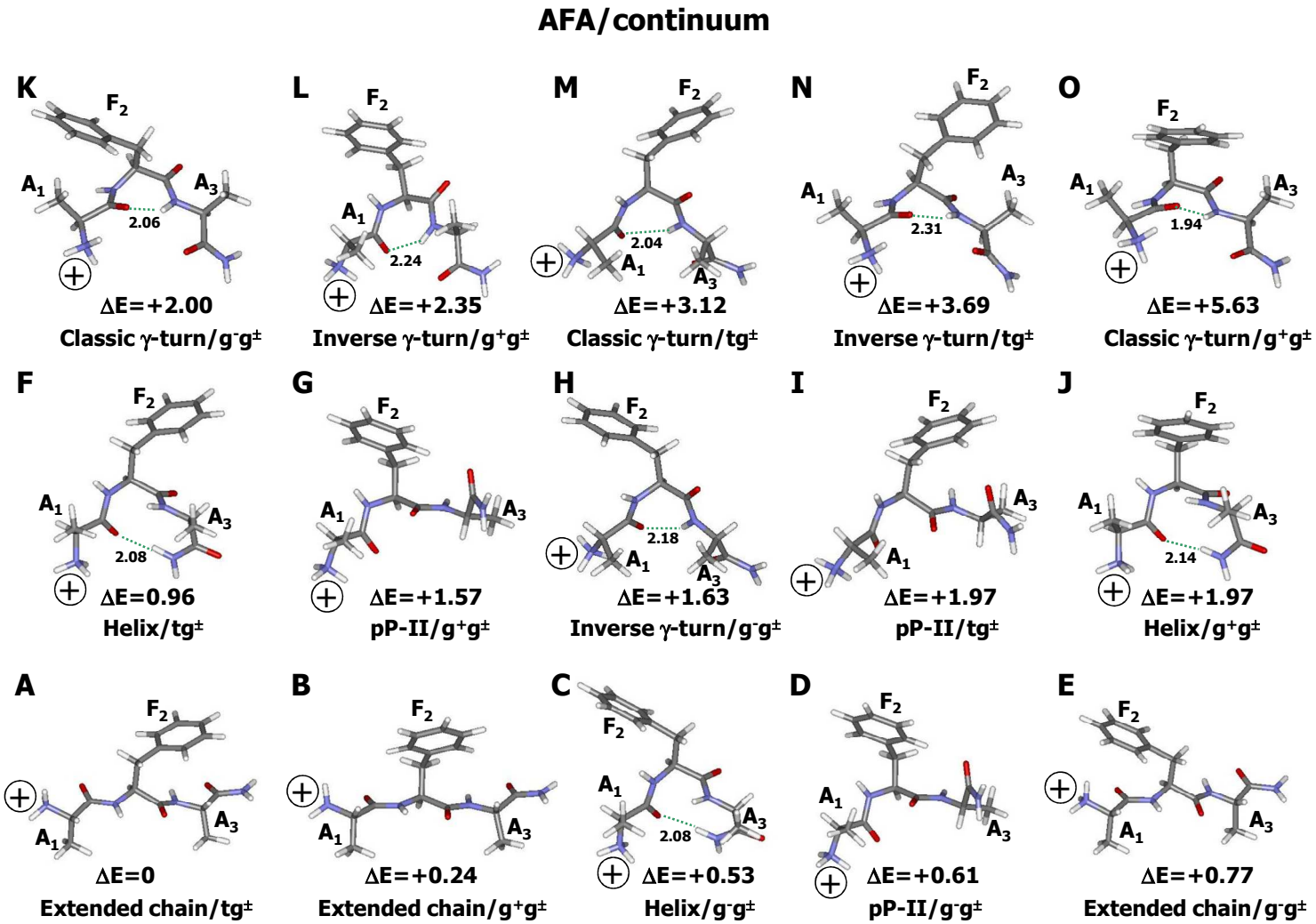

Fig. 5 Graphical representation of the fifteen optimized structures for the AFA cationic species embedded in a polarizable continuum.

From bottom to top the structures are presented in the increasing order of their relative energy (ΔE) as expressed in kcal/mol. $g^+g^\pm$, $g^-g^\pm$ and $tg^\pm$ notations recall the side chain orientation of the middle residue (see text for details). Characteristic intramolecular H-bonds are drawn in broken green lines, of which the length (in Å) is displayed.

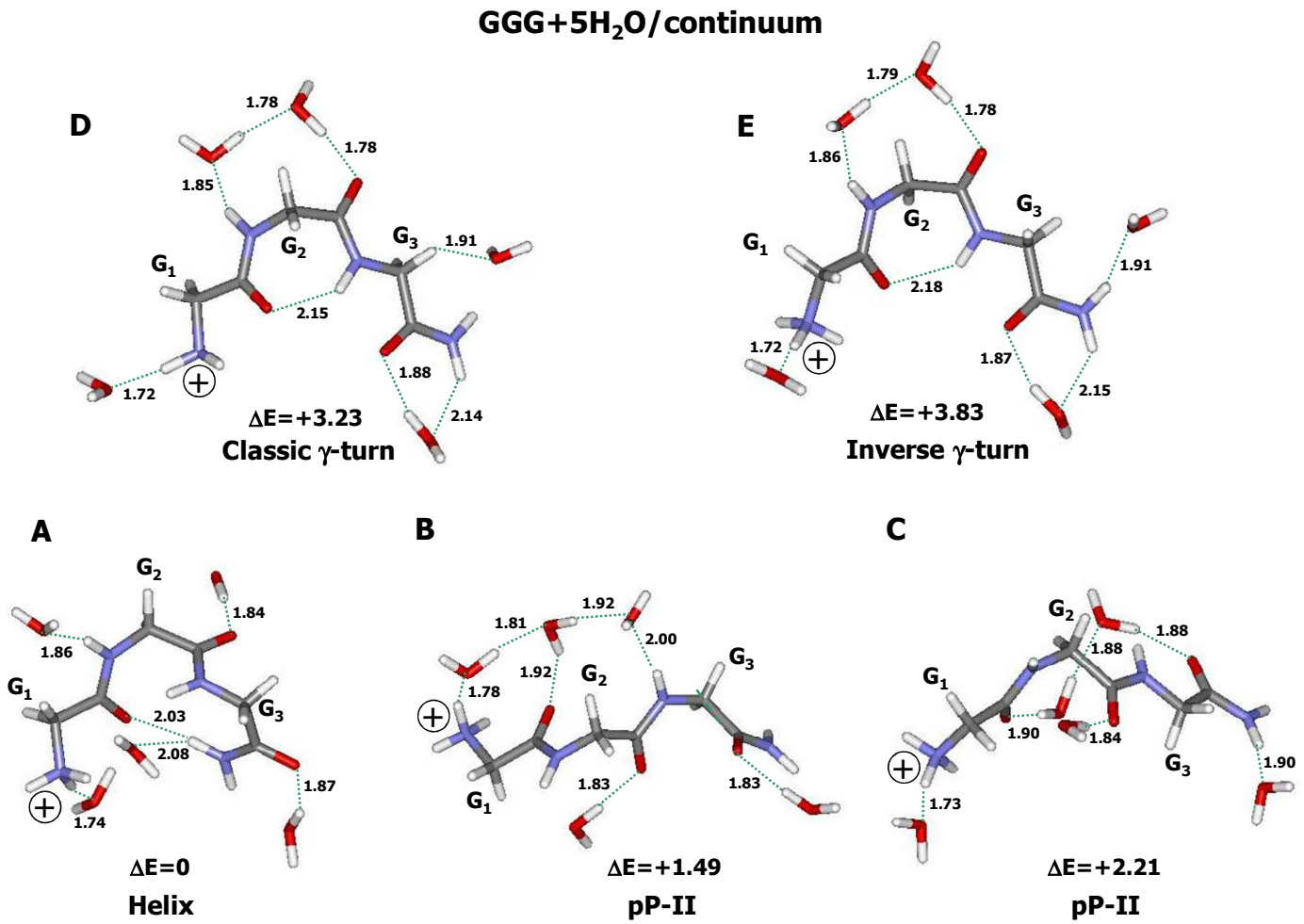

Fig. 6 Graphical representation of the five optimized structures for the GGG+5H_2O clusters embedded in a polarizable continuum.

From bottom to top the structures are presented in the increasing order of their relative energy (ΔE) as expressed in kcal/mol. Characteristic intra- and intermolecular H-bonds are drawn in broken green lines, of which the length (in Å) is displayed.

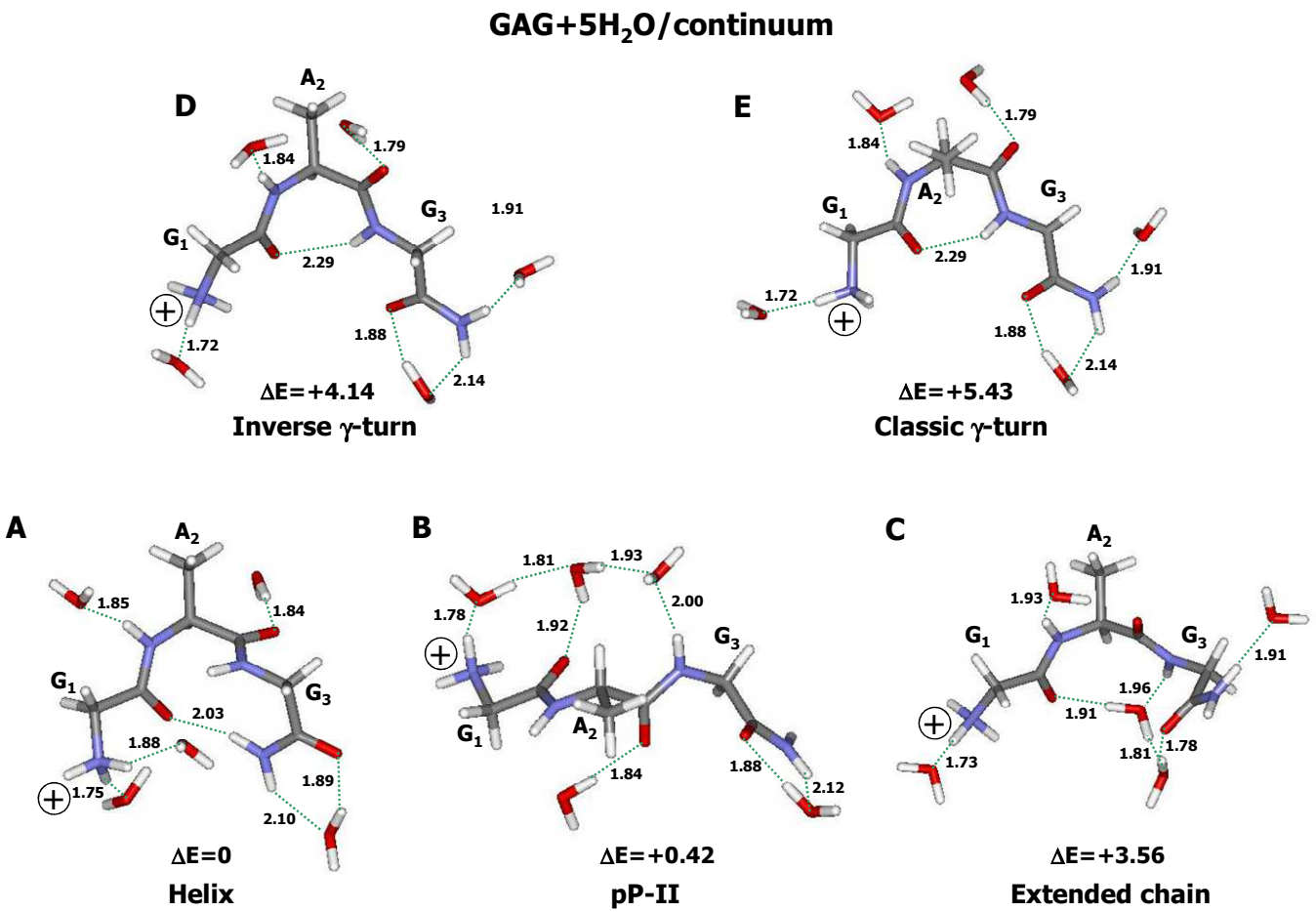

Fig. 7 Graphical representation of the five optimized structures for the GAG+5H_2O clusters embedded in a polarizable continuum.

From bottom to top the structures are presented in the increasing order of their relative energy (ΔE) as expressed in kcal/mol. Characteristic intra- and intermolecular H-bonds are drawn in broken green lines, of which the length (in Å) is displayed.

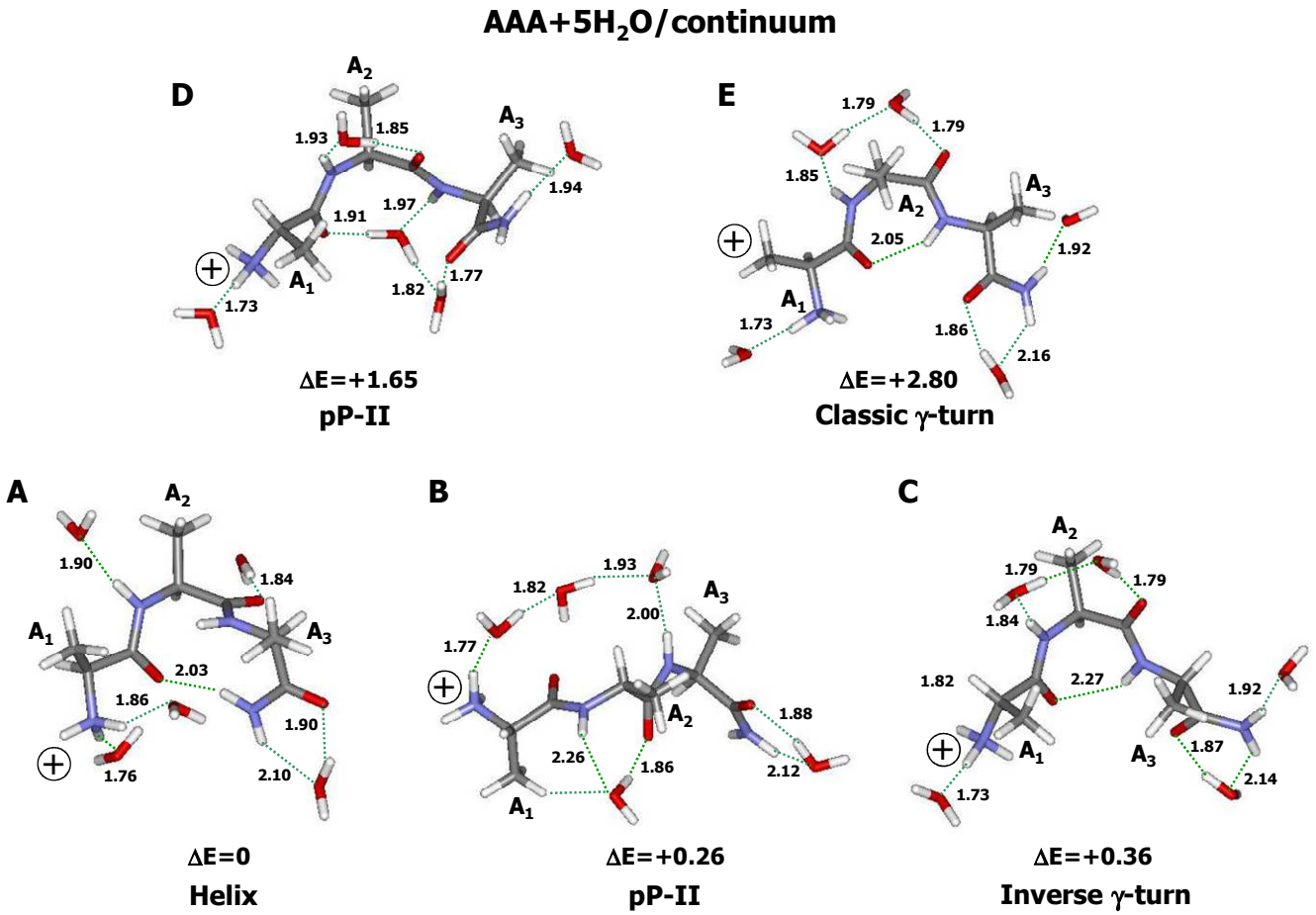

Fig. 8 Graphical representation of the five optimized structures for the AAA+5H_2O clusters embedded in a polarizable continuum.

From bottom to top the structures are presented in the increasing order of their relative energy (ΔE) as expressed in kcal/mol. Characteristic intra- and intermolecular H-bonds are drawn in broken green lines, of which the length (in Å) is displayed.

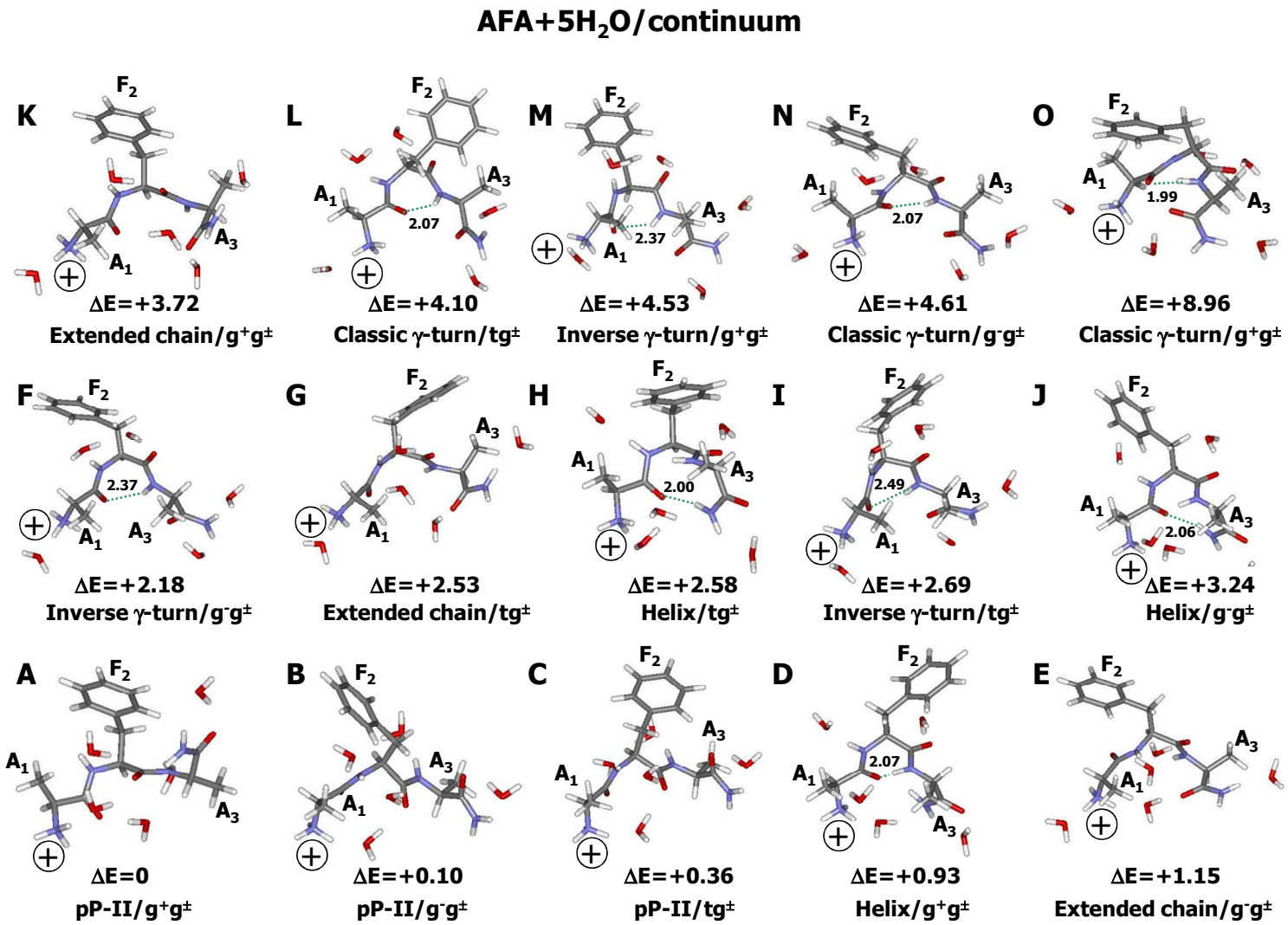

Fig. 9 Graphical representation of the fifteen optimized structures for the AFA+5H_2O clusters embedded in a polarizable continuum.

From bottom to top the structures are presented in the increasing order of their relative energy (ΔE) as expressed in kcal/mol. For the sake of clarity, only the intramolecular H-bonds are drawn in broken green lines, of which the length (in Å) is displayed. The intermolecular H-bonds are very close to those found in AAA+5H_2O (Fig. 8).

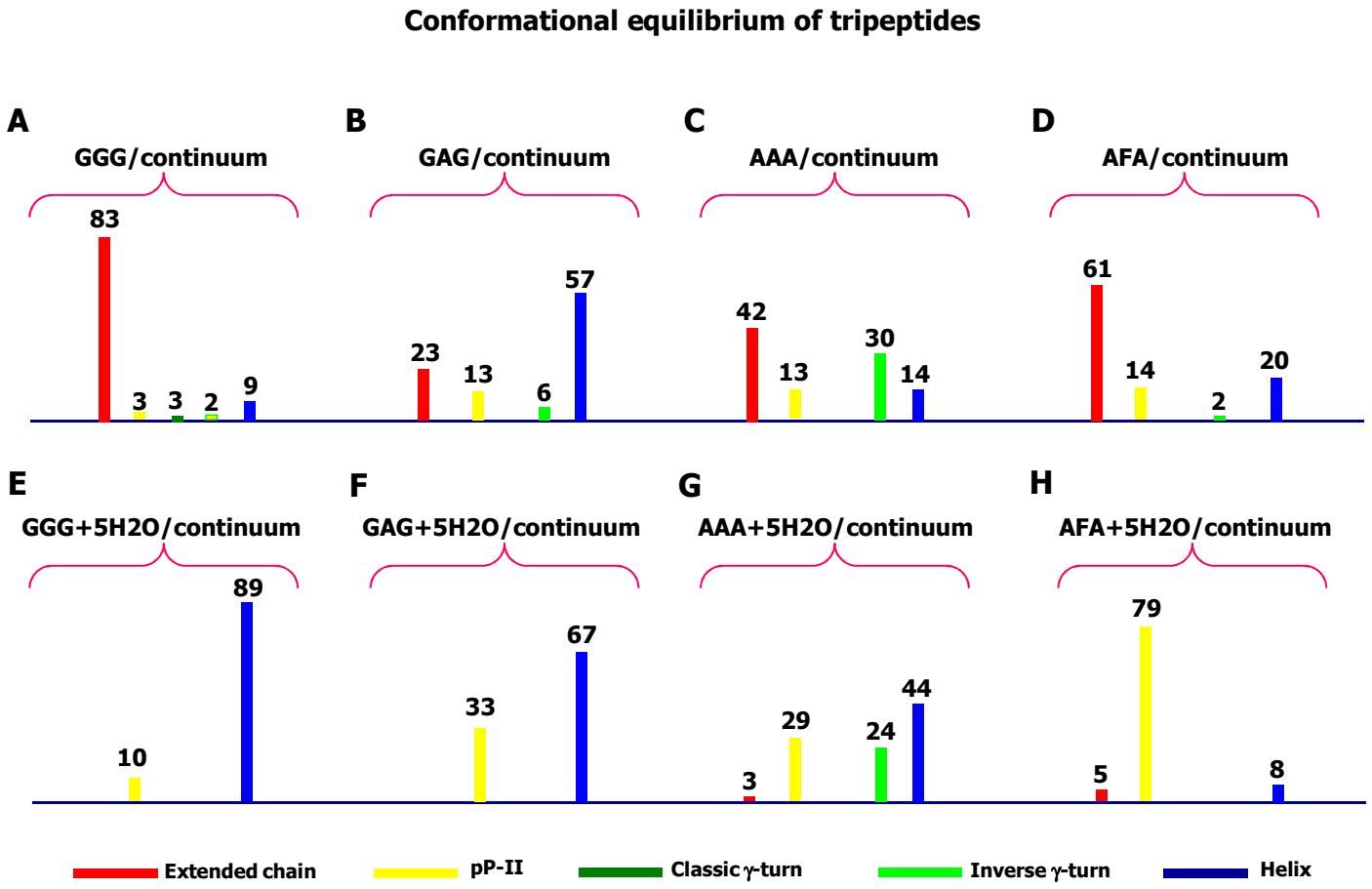

Fig. 10 Histograms representing the normalized Boltzmann thermal weights for the five analyzed secondary structure. Above each bar the value of the thermal weight as expressed in percent is reported. Only the weights ≥1% were displayed.

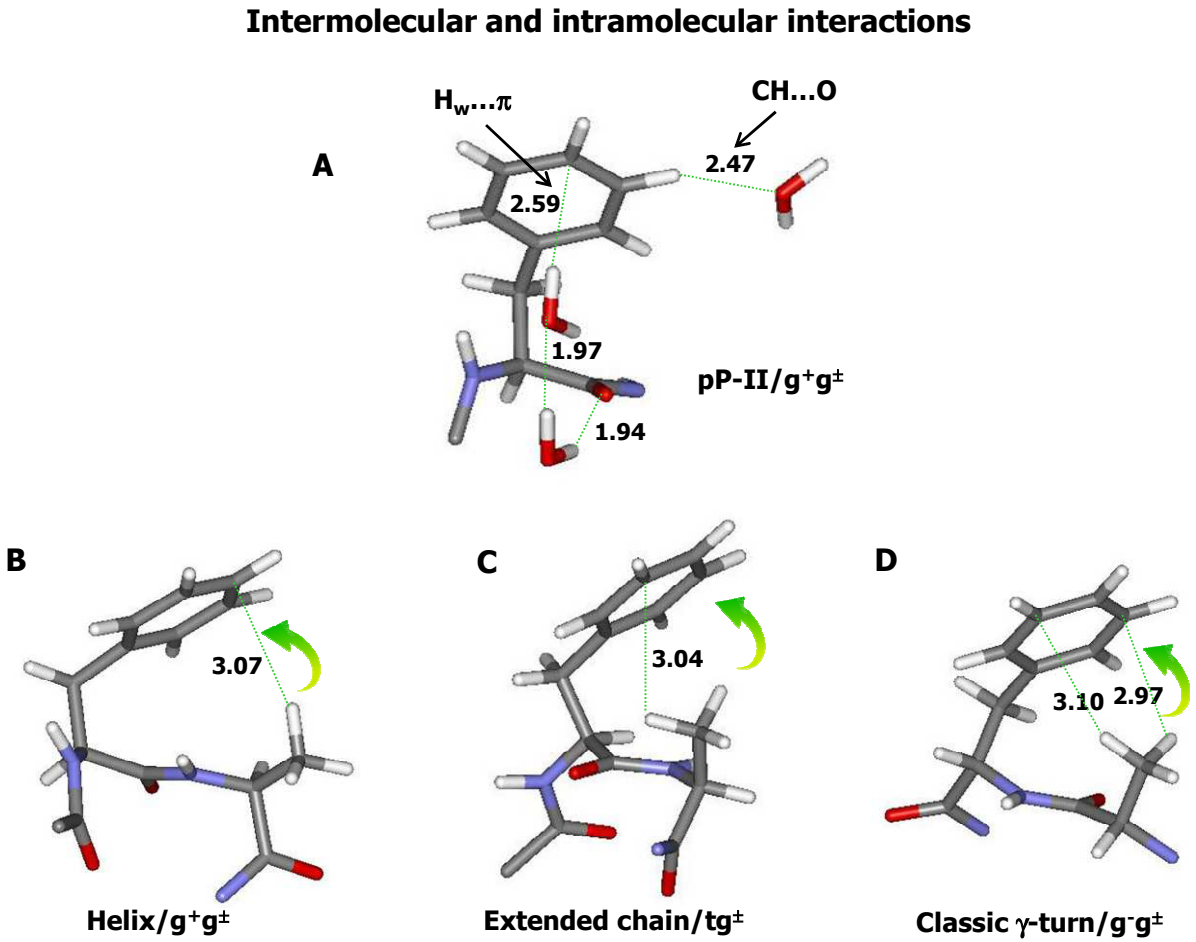

Fig. 11 Graphical representation intramolecular and intermolecular interactions evidenced by in AFA.

(A) H_W... π interaction between the water molecule and the phenyl ring. (B-D) aliphatic-aromatic interactions between the adjacent Ala and Phe residues. H-bonds are drawn in broken green lines, of which the length (in Å) is displayed. Backbone conformation and side chain orientation are also indicated below each case.

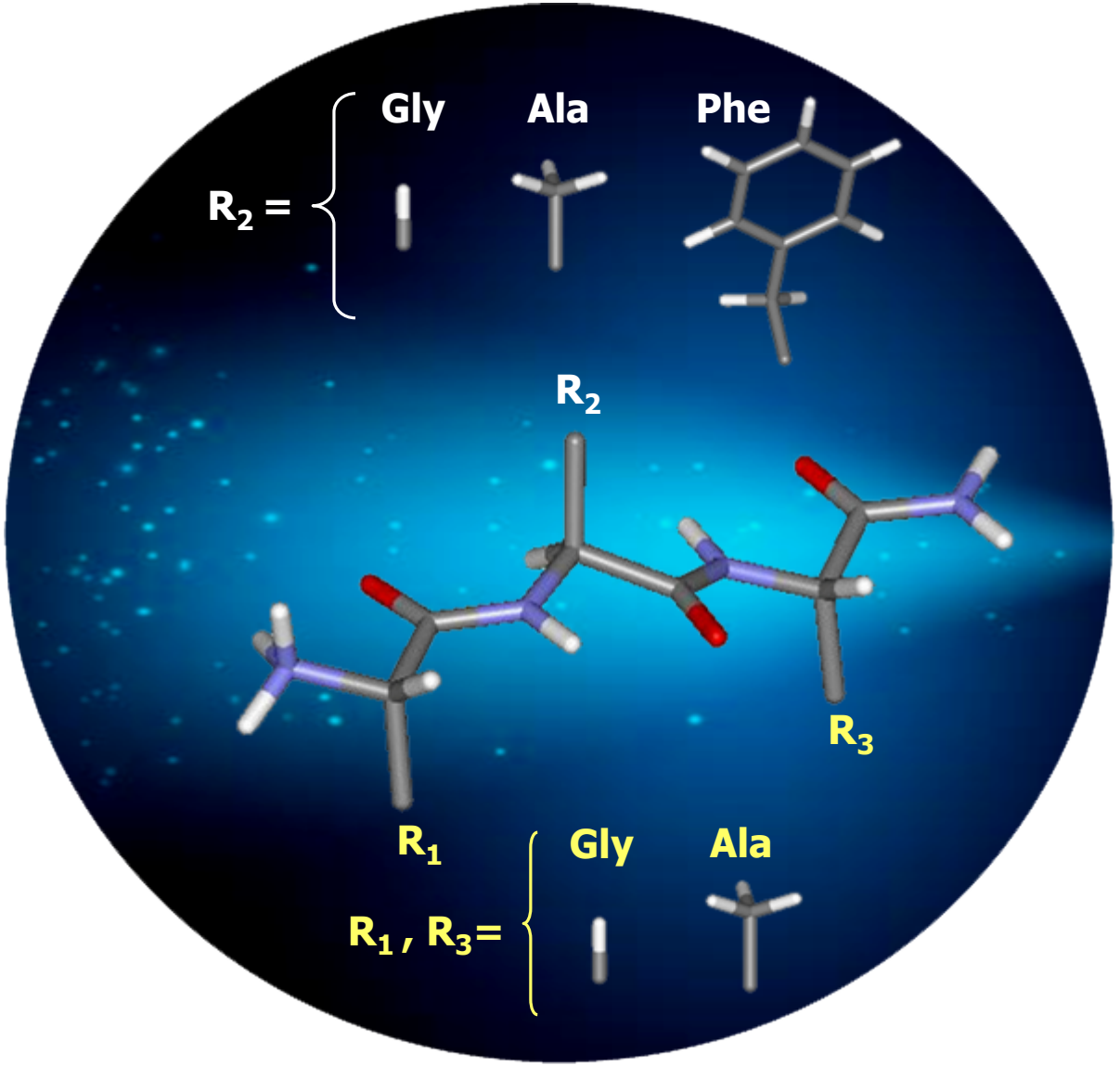
Gly
Ala
Phe
R2 =
R2
R3
R1
Gly
Ala
R1 , R3=